Department of Veterans Affairs

JRRD Volume 41, Number 3A, Pages 325–336
May/June 2004
Journal of Rehabilitation Research & Development

Image-shifting optics for a nystagmus treatment device

Ryan M. Smith, BSEE; Brian S. Oommen, MS; John S. Stahl, MD, PhD
Departments of Neurology, Louis Stokes Cleveland Veterans Affairs Medical Center and Case Western Reserve University, Cleveland, OH

Abstract—Acquired pendular nystagmus (APN) complicates multiple sclerosis and other neurological disorders, causes visual impairment, and is often refractory to available treatments. Vision could be improved by an optical aid that shifts the seen world in lockstep with the APN. An essential component of such a device is the image-shifting mechanism, which must be light, accurate, suitable for battery operation, and capable of image shifting at the frequencies and amplitudes seen in APN. We determined that a three-lens image-shifting mechanism used in commercial image-stabilizing lenses has the potential to satisfy all these requirements. In combination with software designed to track nystagmus, the optical mechanism proved capable of improving visual acuity in 12 normal subjects experiencing simulated two-dimensional nystagmus. Acuity was restored to within an average of 0.12 logMAR (range 0.0–0.22) of the subjects' values without the simulated nystagmus. These results support the feasibility of an assistive device for patients with APN.

Key words: adaptive filter; adaptive optics; demyelination; image stabilization; multiple sclerosis; nystagmus, pathological; oscillopsia; visual acuity.

INTRODUCTION

Acquired pendular nystagmus (APN) is an involuntary, sinusoidal oscillation of the eyes that produces the illusion that the world is in motion (oscillopsia) and degrades the clarity of vision [1]. It appears as a complication of multiple sclerosis and stroke, as well as other disorders that damage the cerebellum or its connections. APN is difficult to treat. While numerous medications have been reported to help selected patients, efficacy and tolerability are frequently unsatisfactory in general practice. Weakening eye muscles can attenuate the nystagmus, but impair the normal eye movements as well [2]. Acuity in APN patients can be improved by devices that sense eye movements and optically shift the image of the world in lockstep with the moving retina [3,4]. Such devices can be contrived so as to counteract the nystagmus selectively, minimizing interference with normal eye movements [4]. We have recently demonstrated a particularly effective method of achieving this selectivity, using a computer-based filter known as an adaptive interference canceller [5,6].

In order to be useful to patients in their daily lives, a nystagmus visual aid should be self-contained, battery-operated, and portable. These goals are relatively easy to achieve for some of the components of the device. For instance, while we have, to date, implemented the adaptive filter software on a desktop computer, it is well-suited for implementation on a portable platform built around a

Abbreviations: APN = acquired pendular nystagmus, CCD = charge-coupled device, FFT = fast Fourier transform, I/O = input/output, PID = proportional integral derivative, RMS = root-mean-square, THD = total harmonic distortion, VOR = vestibulo-ocular reflex.

This material was based on work supported by a Rehabilitation Research and Development award from the Department of Veterans Affairs.

Address all correspondence to Dr. John S. Stahl, Department of Neurology, University Hospitals of Cleveland, 11100 Euclid Avenue, Cleveland, OH 44106-5040; 216-844-3170; fax: 216-844-5066; e-mail: jss6@po.cwru.edu.

digital signal processor. Moreover, most of the activities the device would be used to facilitate (e.g., reading) are sedentary, and as such the utility of the device would be hardly compromised if its power supply and control circuitry were table-, wheelchair-, or scooter-mounted as opposed to actually wearable. In contrast, the image-shifting optics must be wearable, and represent more of a technological challenge. In our previous study of the potential benefits of selective nystagmus compensation in APN patients, image shifting was accomplished with the use of motorized Risley prisms [4]. A Risley prism consists of a pair of circular wedge prisms paired base-to-apex, geared so that rotation of one prism causes its fellow to rotate in the opposite direction. Each prism pair is capable of translating images along one axis. Unfortunately, a Risley arrangement capable of two dimensions of image shifting is inherently unsuitable for a wearable device. Its four prisms and intervening gearing amount to a very long assembly, which is difficult to support on the head due to weight and mechanical leverage, and affords an excessively narrow field of view for any reasonably sized prisms. The gearing mechanism introduces mechanical backlash, degrading the fidelity with which the device responds to its command signals. Gears are noisy and likely to wear rapidly under the continuous, to-and-fro rotation to which they would be exposed in a nystagmus compensating device. Finally, the geared prism arrangement requires relatively powerful motors. In our prototype, we required two high-performance stepper motors, each weighing 200 gm and capable of 0.16 N-m of torque. The weight, power consumption, and heat dissipation requirements of such motors are incompatible with a wearable device.

There are a number of alternatives to image shifting with Risley prisms, many of which are exploited in image-stabilizing photo-optical products [7]. One approach used in camcorders involves focusing the scene on an oversized charge-coupled device (CCD) and then electronically shifting the image by remapping it within its raster. In a nystagmus compensating device the stabilized image would then be displayed on a head-mounted screen, analogous to that used in virtual-reality goggles. This approach is attractive because it does not require moving parts, and unlike most optical mechanisms, could compensate for torsional as well as horizontal and vertical oscillations. However, the patient would view the world indirectly through a television camera, and obtaining clear images of finely detailed objects (e.g., a printed page) would likely require inconvenient adjustments for focus and luminance. Another approach is to use electromagnetically steered mirrors. Mirror arrangements are attractive in that they can convert relatively tiny physical movements into large angular displacements of the image, and thus may be driven by small, energy-efficient actuators. However, like the CCD arrangement, they would afford the patient only an indirect view of the world, as through a periscope.

Two types of image-shifting devices provide a direct view of the world, thereby avoiding some of the drawbacks of the CCD or moving mirror arrangements. The variable angle prism developed by Canon, Inc., and employed in that company's line of image-stabilized binoculars consists of two glass elements connected by a flexible envelope filled with optically clear oil. The glass elements are steered by miniature motors, thereby modifying the prismatic power of the assembly. Another mechanism, used in Canon's image-stabilized lenses for 35 mm cameras, consists of three lenses, the middle of which is electromagnetically shifted to control the magnitude of image deflection. This second arrangement is particularly suitable for use in a wearable nystagmus compensating device. It is particularly compact, since there is only one moving element whose motion is confined to the plane perpendicular to the optical axis, allowing the three lenses to be sandwiched tightly. Moreover, relatively small forces are required to translate the single lens, allowing for the use of tiny motors with low current draws and little potential for problems related to heat dissipation.

In the current study we explored the potential for the three-lens arrangement to serve as the image-shifting component of a visual aid for patients suffering from APN. We assessed the power requirements and accuracy of a mechanism built from parts extracted from a commercial image-stabilizing photographic lens and tested its ability, when coupled to our computer-based adaptive interference canceller [6], to restore acuity in normal subjects in whom the deleterious effects of APN were simulated by oscillating visual targets.

METHODS

Subjects

The experimental protocol was approved by the Institutional Review Board of the Cleveland Veterans Affairs Medical Center, and all subjects gave informed consent. We studied 12 subjects, aged 23 to 51 years. Subjects

were neurologically and neuro-ophthalmologically normal. Seven subjects customarily wore correction, and did so during testing (three subjects wore spectacles, three wore contacts, and one wore spectacles for one session and contacts for a second session).

Image-Shifting Optics and Associated Circuitry

The operation of a three-lens image shifter as applied to the problem of nullifying the visual effects of eye movements is diagrammed in **Figure 1**. The assembly consists of an electromagnetically steered biconcave lens sandwiched between two stationary lenses. Motion of the central lens shifts the image of the world in the direction of the lens movement. The figure, which we constructed using optical modeling software (Raytrace, IME Software, Toowong, QLD, Australia), demonstrates how a downward motion of the lens deflects the light rays upward, thereby maintaining the original focus point upon the fovea despite the 5° downward rotation of the eyeball.

We purchased a commercial image-stabilizing zoom lens (EF 28-135 mm, Canon Inc., Japan) and disassembled it to obtain the central components of its three-lens image-shifting device, including the biconcave lens, the moving mounting/armature, and the driving voice coils (electromagnets). The armature also carries a pair of surfaces (one for each axis of lens movements) whose darkness/reflectivity varies continuously from one side to the other. In combination with an infrared emitter/detector pair, these surfaces form an optical position sensor, the output of which is proportional to the position of the armature along the axis of the reflectivity gradient, but insensitive to any motion in the orthogonal direction.

The product's voice coil drivers and infrared emitter/detector pairs were enmeshed in proprietary multifunction circuitry and thus not conducive to modification. Consequently, we removed all the original electronics. We assembled replacement emitter/detector pairs (GP2S09, Sharp) on a circuit board and joined the board to the lens support. We machined a plastic housing, into which we mounted the assembly. The assembly was oriented to place the two orthogonal motion axes at 45° to the vertical, thereby causing the two voice coils to share equally the burden of supporting the lens against gravity. The portion of the housing that, in use, would be directed away from the patient's eye was machined to accommodate a 25 mm diameter, 100 mm focal length, plano-convex objective lens (LA1509, Thor Labs). The patient side of the housing mounted the 25 mm diameter, 125 mm focal length, biconvex ocular lens

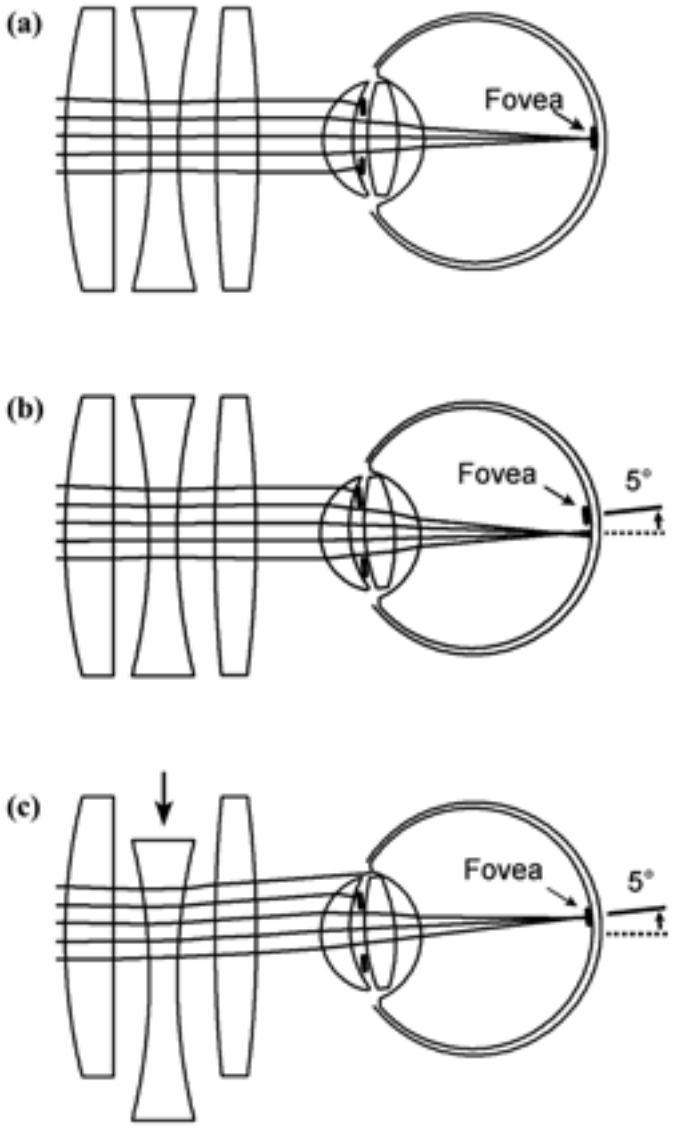

Figure 1.
Demonstration of operation of 3-lens image-shifting device applied to problem of nullifying visual effects of eye movements: **(a)** Initial condition with eye and optics in neutral positions. Light rays emanating from distant visual target (not shown) are brought to focus on the fovea. **(b)** Eye is rotated 5° downward, displacing image of visual target from fovea. **(c)** Central lens of optical device is moved downward, shifting light rays and realigning focus point with fovea.

(LB1904). Together, the three-lens assembly achieved approximate unity magnification, and was capable of displacements of the visual world up to approximately ±1.4° in horizontal and vertical directions. The ocular side of the housing also incorporated an ultra-miniature television camera measuring 9 mm in height and width and 18 mm in depth (EC-605, ISCAN, Burlington, MA) mounted in a

ball-and-socket configuration, as well as two infrared illuminators (PDI-E801, Photonic Detectors, Simi Valley, CA). Finally, the entire assembly was mounted to an adjustable headband salvaged from a low-cost face shield. The completed unit and a close-up of the image-shifting assembly are shown in **Figure 2**. It afforded subjects a clear field of view measuring approximately ±6°.

We constructed a linear voice coil driver circuit based on a power operational amplifier chip (LM675, National Semiconductor). The completed circuit was potentially capable of driving inductive loads at currents up to 3 A, although practically it was limited to 300 mA by our breadboard's power supply. An additional circuit was constructed to condition the output of the optical position sensor. Based on a quad operational amplifier (LM324, National Semiconductor), the circuit biased and amplified the photodetector output to a range useful for the analog-to-digital converters in a desktop computer. The power driver and the photodetector circuits were interfaced to the personal computer running the control software via a multifunction analog input/output (I/O) board (PCI-MIO-16XE-10, National Instruments). Eye position was extracted from the output of the ultra-miniature video camera with a separate personal computer containing pupil-tracking hardware and software (RK-726PCI, ISCAN, Burlington, MA). The ISCAN system output analog signals proportional to horizontal and vertical eye position, which were input to the control computer via its analog I/O board.

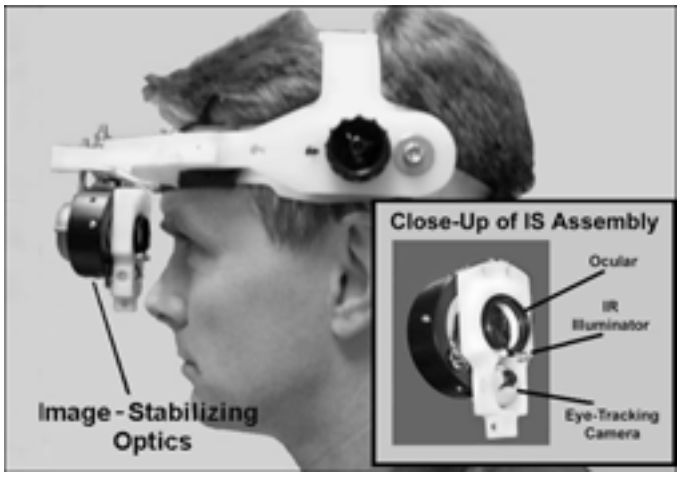

Figure 2.
One author models completed head-mounted nystagmus-compensating device. Inset: Close-up of front (ocular) side of optics, showing ocular fixed lens, infrared (IR) light sources, and ultra-miniature eye-tracking camera in its ball-and-socket joint.

Control Software

Control software was implemented on the desktop "control" computer in Real-Time Simulink (The MathWorks, Natick, MA) running on a Microsoft Windows 2000 platform. Central to this software was an adaptive interference cancellation filter, which generated a sinusoidal waveform whose amplitude, phase, and frequency matched the sinusoidal nystagmus waveform [5,6]. This nystagmus replica drove the image-shifting optics, causing the image of the seen world to shift with the nystagmus and thereby nullifying the visual effects of this involuntary movement. The filter conferred specificity upon the device, causing it to nullify the involuntary movements while largely "ignoring" normal eye movements.

The software also accomplished additional tasks. Prior to entering the adaptive filter, the eye movement signals (vertical and horizontal) passed through software that detected interruptions in the eye-tracking signal. Such interruptions were usually caused by the subject blinking, and the associated large positive or negative voltages output from the ISCAN pupil tracker tended to cause the active optics to "jump" to their mechanical limits. The software detected the tracking loss based on the input's sudden swing to an extreme positive or negative value and clamped the input to zero (thus stilling the optics) for the duration of the transient. An additional benefit of this tracking loss feature was that it automatically disabled the optics whenever the headset was removed from the subject. The software also accounted for the difference between the axes used by the eye tracker (i.e., horizontal and vertical with respect to the inter-ocular axis), and the optics voice coils (which operated in a reference frame rotated 45° from the vertical). This coordinate transfer was accomplished by passing the outputs of the horizontal and vertical channels of the filter through a rotation matrix. Finally, the Simulink software also closed the feedback loop of the voice coil driver circuit. **Figure 3** shows a block diagram of this segment of the code, which is configured as a proportional-integral-derivative (PID) servo. Note that the servo control software includes an adjustable gain for each axis of the image-shifting optics. The gains are adjusted during the experiment as described below.

Assessments of Device Accuracy

The fidelity of the device (degree to which the motion of the moving lens matched the command signals) was assessed by calculating total harmonic distortion (THD) in each motion axis and root-mean-squared

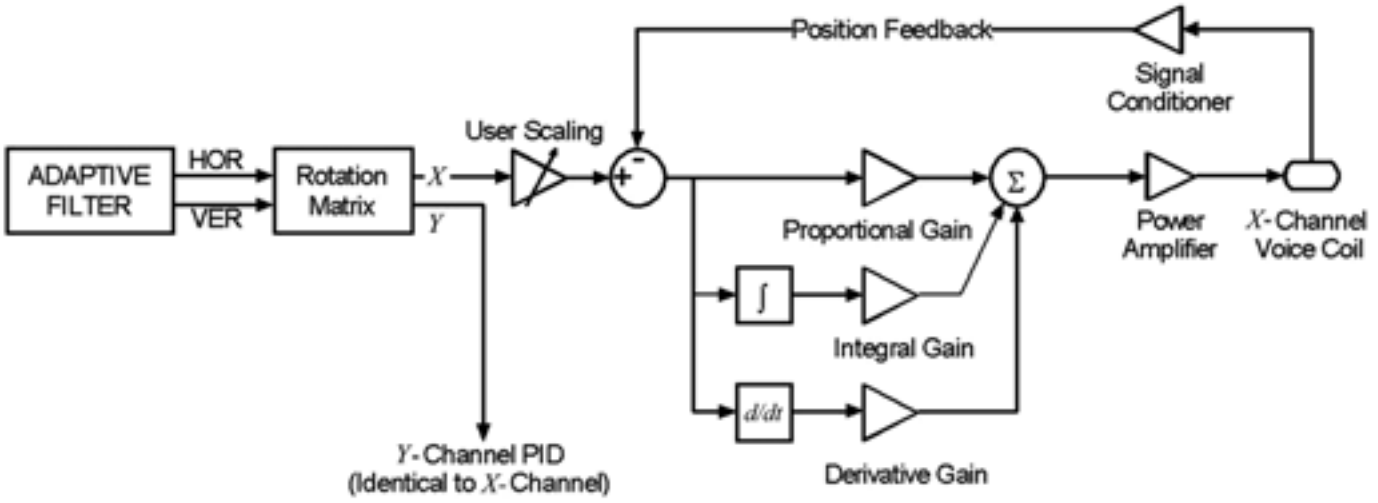

Figure 3.
Block diagram of Simulink code implementing PID control of optics voice coils. There are two voice coils (one for each axis of motion), and because controllers for each coil are identical, only one is diagrammed. Note that command signal to both channels originates from sinusoidal outputs of adaptive filter. Gain factor in each channel is adjusted at outset of each session so as to nullify apparent motion of oscillating test figure.

(RMS) error of the (2D) lens trajectory. Both calculations were based on a 5 s sample of the command and lens position feedback signals obtained at a sampling rate of 200 Hz as the device was driven in a circular trajectory at various rates. THD for either axis of the device was calculated from the fast Fourier transforms (FFTs) of the input (command) and output (feedback) waveforms from either device axis as

$$100\% \times \sqrt{\frac{\text{sum}[(A_{\text{OUT}}[i] - A_{\text{IN}}[i])^2]}{\text{sum}(A_{\text{IN}}[i]^2)}} \qquad (1)$$

where $A_{\text{OUT}}[i]$ is the amplitude of the ith component of the spectrum of the output signal, and $A_{\text{IN}}[i]$ is the amplitude of the ith component of the spectrum of the input signal. Note that the PID controller was tuned so that the output and input amplitudes were approximately equivalent at the selected test frequencies. As such, $A_{\text{OUT}}[i] = A_{\text{IN}}[i]$ at the spectral element corresponding to the test frequency, and the sum in the numerator represents simply the sum of the squared amplitudes at all frequencies other than the test frequency. Since all the spectral power of the input signal is concentrated at the selected test frequency, the denominator simplifies to $A_{\text{IN,TEST}}$, the amplitude at the test frequency.

Device fidelity was also assessed by calculation of the RMS error between the desired and actual 2D paths of the moving lens. RMS error was calculated as

$$\sqrt{\frac{\text{sum}[(Y_O[n] - Y_I[n])^2 + (X_O[n] - X_I[n])^2]}{N}} \qquad (2)$$

where $Y_O[n]$, $Y_I[n]$ are the nth samples of the output and input signals in the Y direction, $X_O[n]$, $X_I[n]$ are the nth samples of the output and input signals in the X direction, and N is the total number of samples. Note that the X and Y directions refer to the motion axes of the device, which are rotated 45° to the horizontal/vertical coordinates used by the pupil tracker and the nystagmus tracking filter.

Visual Stimuli, Nystagmus Simulation

Acuity testing was accomplished as described in the previous study [6]. Briefly, acuity testing figures consisted of eight-position Landolt C characters (optotypes), with each test optotype being presented as the central element of a 3 × 3 grid of optotypes. The test and surrounding distractor optotypes were scaled to range from 30 ft to 6 ft sizes in 0.1 logMAR steps. At our viewing distance of 10 ft, this range corresponds to decimal acuity chart sizes of 0.33 to 1.7, and a logMAR range of +0.48 to –0.23 (a range of approximately eight lines on the Bailey-Lovie logarithmic acuity chart, in which adjacent

lines differ by 0.1 logMAR [8]). Each test block consisted of a randomized set of 24 optotypes of a single size, with each of the 8 possible orientations occurring 3 times. Test figures were projected on a white screen by a digital projector. During testing, each optotype was presented to the subject for 4 s.

As in the previous study [6], we tested normal subjects in whom the visual effects of nystagmus were simulated by oscillating the acuity test figures. The oscillation was achieved by relaying the projection through a pair of mirror galvanometers (model CX660, General Scanning), configured to deflect the image in horizontal and vertical directions. In the current experiments, the image was always driven in a circular trajectory, with a repetition rate of 4.5 Hz and a radial amplitude of 0.6°. This amplitude was dictated by the performance of the image-shifting optics, the fidelity of which declined when driven too near the excursion limits of the moving lens element. Note that this amplitude is somewhat smaller than that tested in the previous study, which employed *simulated* image-shifting optics [6].

In a subset of subjects we verified that the operation of the device did not degrade vision during the execution of normal gaze-shifting eye movements. In these experiments acuity was assessed as the acuity test patterns moved in two alternating trajectories—two revolutions about a circular path (which required that the subject use smooth pursuit to maintain fixation) and jumping twice around the four points of a square (requiring that the subject execute saccades). The circular trajectory measured 0.6° in radius and each revolution was completed in 4 s, while the square trajectory measured 0.6° on a side, and a circuit was completed in 4 s, with the target remaining at each stable position for approximately 1.0 s (i.e., transitions between the points of the square trajectory were, effectively, instantaneous). Only the subjects' eye movements were fed into the adaptive filter software. Unlike the stabilization experiment, we did not add the command signals to the mirror galvanometers. The difference in the filter inputs stems from the fact that in the stabilization experiment, we needed to add the oscillation to simulate the presence of the involuntary nystagmus "riding" on desired eye movements, whereas in the specificity experiment we needed to assess only the response of the filter to actual pursuit and saccade eye movements.

Experimental Procedure

All subjects were tested with the image-shifting assembly mounted in front of one eye and an occluder positioned over the fellow eye. We began the experimental sessions by fitting the optics headset to the subject and adjusting the position of the integral video camera so as to achieve reliable pupil tracking. Next, the horizontal and vertical optics gain factors (see **Figure 3**) were adjusted in turn as subjects viewed a single bright spot moving in the 4.5 Hz, 0.6° amplitude circular trajectory. Horizontal gain was increased until the spot appeared to be moving in a vertical line (i.e., horizontal motion was nullified). Then vertical gain was adjusted (with the horizontal channel of the optics turned off) until the spot appeared to be moving in a horizontal line.

Once the adjustments were completed, we tested acuity with the acuity charts stationary and the optics off ("baseline acuity condition"), with the acuity charts in motion and the optics off ("untreated condition"), and with the acuity charts moving and the stabilizing optics on ("treated condition"). The test battery required approximately 15 min to complete, and all but two subjects were tested twice, with testing sessions separated by hours to days. As noted above, five subjects were tested in an additional session in which the optics were either enabled or disabled while acuity test charts moved alternately in trajectories requiring fixation be maintained using saccades and smooth pursuit (the "optics enabled saccade/pursuit" and "optics disabled saccade/pursuit" conditions, respectively). For each condition, we began with larger character sizes and progressed to smaller sets until subject accuracy fell below 13/24 characters or, equivalently, 54 percent (the midpoint between perfect and chance performance). To further reduce the number of optotype sets we needed to test, we roughly identified the subset of sizes over which subject accuracy declined, with the help of a ranging set consisting of 5 characters of each size. In practice, we only needed to perform ranging in the treated condition, since the appropriate range of target sizes for the baseline acuity condition could be inferred from the performance in the treated condition, and no subject was able to identify any characters in the untreated condition. Subjects were given a brief rest between each stimulus condition. Subjects were instructed to indicate the orientation of each optotype as it displayed. The responses were entered into a Microsoft Excel spreadsheet, which automatically compared the responses to the correct sequence and tabulated the number of correct responses for each condition.

Data Analysis

Acuity was determined in each condition as described in the previous study [6]. Briefly, for each subject and condition, we averaged the number of correct responses at each optotype size over the two testing sessions. (Two subjects underwent only a single testing session and in those cases no averaging could be performed.) We then plotted average number correct versus optotype size, expressing optotype size as it would appear on a decimal acuity chart, e.g., 5 ft letters at a viewing distance of 10 ft would correspond to a 2.0 line on a decimal acuity chart. We fit each accuracy curve with a sigmoid curve and defined the subject's acuity as the value at which the fitted curve fell below our criterion level of 13. Note that throughout, acuities are variously expressed as ratio, decimal, or logMAR as is most convenient in the particular context. All average values are given as mean ± standard deviation.

RESULTS

Mechanical Performance

The image-shifting optics exhibited a number of features rendering them particularly suitable for application in a nystagmus compensating device. When oscillated so as to nullify the 4.5 Hz, 0.6° circular motion of the acuity test figures, they were virtually silent. The voice coils remained cool to the touch even after prolonged (1 h) operation, indicating that, from the standpoint of heat generation, the apparatus would be appropriate for continuous duty without the need for elaborate heat sinks (which would invariably increase the weight of the completed device).

The performance of the image-shifting optics was characterized in terms of variations in current consumption, THD, and RMS error as functions of oscillation frequency or amplitude. Current consumption was determined by measuring voltage drop across a 1 Ω resistor placed in one of the voice coil power leads. **Figure 4(a)** plots current consumption for one voice coil as oscillation frequency was varied from 0 to 9 Hz with amplitude fixed at the excursion appropriate to nullify a 0.7° oscillation of the acuity figures. Current consumption never exceeded 42 mA and was only weakly related to oscillation frequency over the entire tested range. Note that since 35 mA was required to maintain the optics stationary at their central position (0 Hz data point in **Figure 4(a)**); most of the power consumption in the moving condition related to generating the forces required to support the lens against the pull of gravity. **Figure 4(b)** plots current consumption of one voice coil as the amplitude of the circular oscillation was varied from 0.14 to 1.1° at a fixed rotation rate of 4.5 Hz. Current consumption increased roughly linearly

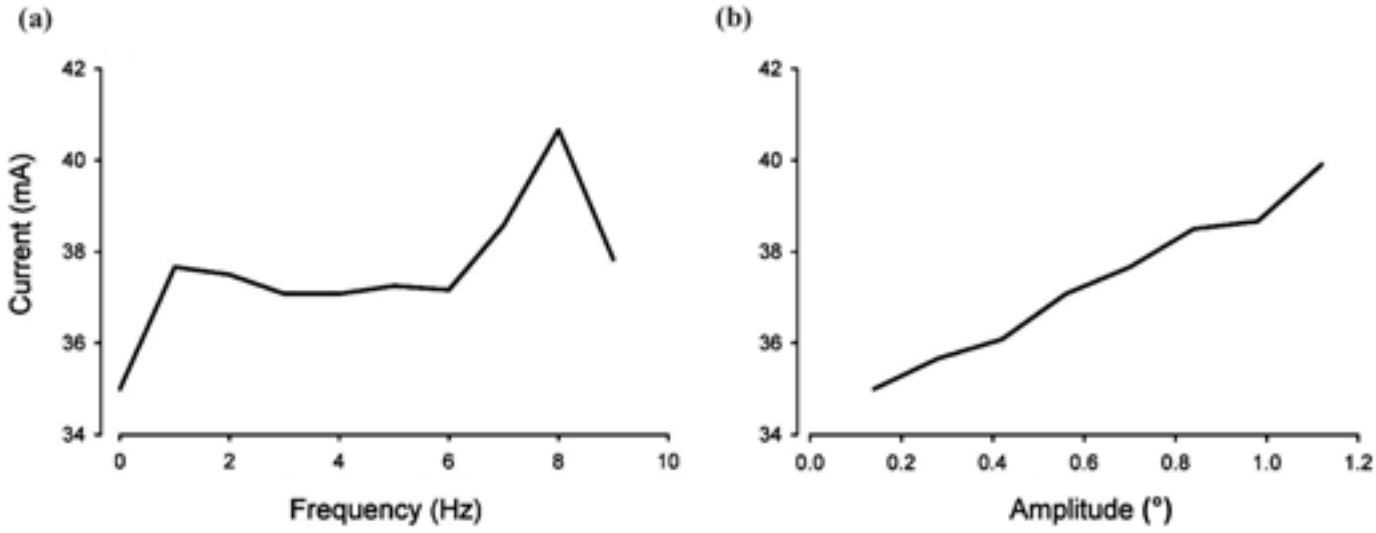

Figure 4.
Current consumption of one of two voice coils of image-shifting optics during stabilization of optotypes moving in circular trajectory: **(a)** current consumption as function of oscillation frequency at fixed oscillation amplitude and **(b)** current consumption plotted as function of oscillation amplitude at fixed oscillation frequency.

with oscillation amplitude, ranging from 35 to 40 mA over the tested amplitude range. Again, the small change in current across the tested amplitude range indicates that supporting the lens against gravity, rather than oscillating the lens, was responsible for the bulk of the current consumption by the voice coils.

The fidelity of the device was assessed by calculating THD at various oscillation frequencies and a fixed amplitude of 0.7°. **Figure 5(a)** plots THD for one voice coil axis as a function of driving frequency (a similar plot for the other axis [not shown] was qualitatively and quantitatively similar). THD ranged from 5 to 7 percent at oscillation frequencies below 8 Hz and then rose steeply at higher frequencies. THD quantifies the degree to which imperfections in the device electronics and mechanics introduce motions at frequencies other than the desired driving frequency. We also calculated RMS error, which quantifies the radial magnitude of the error between the actual and desired deflection of the image of the world as viewed through the optics. **Figure 5(b)** plots RMS error as a function of driving frequency. As with THD, RMS error is fairly flat over the frequencies seen in APN, never exceeding 0.08°. The insets in **Figure 5(b)** show the 2D trajectories of the optics at oscillation frequencies of 1 and 14 Hz. The increasing RMS error values at the higher oscillation frequencies correspond to the trajectory becoming increasingly noisy (thus thickening the trajectory) and less perfectly circular.

Figure 6 explores in more detail the breakdown of fidelity at high oscillation frequencies. **Figure 6(a)** plots actual and desired positions versus time for each axis of the optics during 14 Hz, 0.7° oscillation. Axes are designated *X* and *Y* so as to correspond to **Equation (2)**. Note that the *X* axis position tends to lag its command signal and overshoot at the turnarounds, while the *Y* axis lags to a lesser degree and overshoots only in one direction. **Figure 6(b)** demonstrates how the errors in each axis translate to the 2D error in the image shift. For each sample in the 5 s data segment, we plotted a line segment originating at the desired position and extending to the actual coordinates reached by the device. The direction of the rotation about the trajectory is clockwise, and the orientations of the *X* and *Y* device axes are indicated. Note how the inconsistent phase lags and overshoots produce the variability and polygonal form of the observed trajectory.

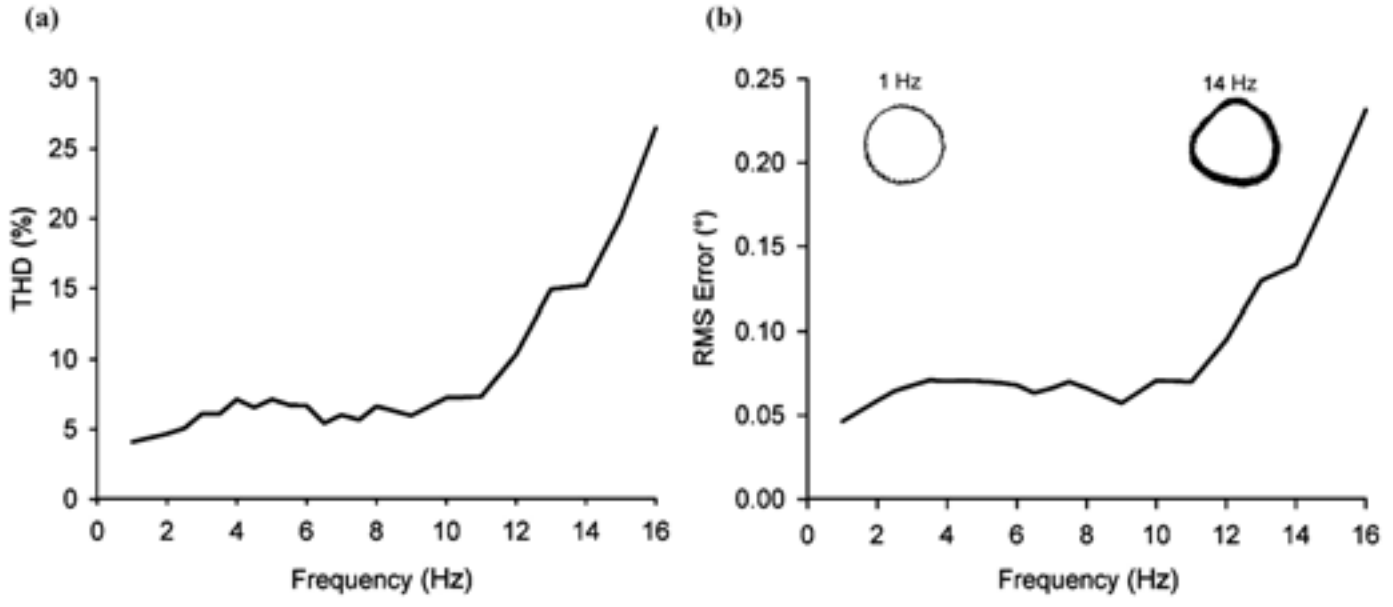

Figure 5.
Measures of degree to which adaptive optics execute desired circular trajectory, plotted as functions of oscillation frequency: **(a)** THD of one axis of device's motion. A 0% THD would indicate perfect fidelity. **(b)** Discrepancy between actual and desired trajectory of image deflection, measured as RMS of 2-D angular deviation between desired and actual positions. Insets show actual trajectories at indicated oscillation frequencies. Both THD and RMS error curves indicate that device fidelity is stable over (and beyond) range of frequencies encountered in APN.

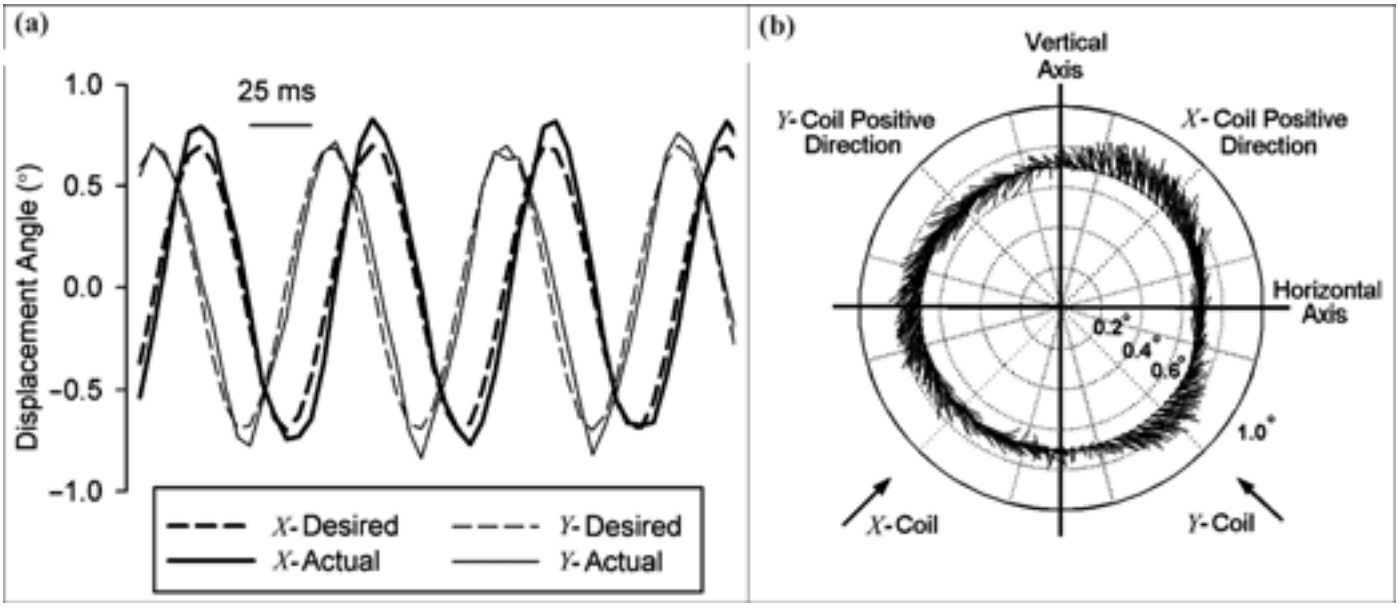

Figure 6.
Exploration of deterioration of device fidelity at higher oscillation frequencies. Both panels were derived from same data, which were obtained at oscillation frequency of 14 Hz and image deflection amplitude of 0.7°. **(a)** Device position versus time for device axes *X* and *Y*. Desired (commanded) positions are superimposed as dashed lines. Actual positions variously lag and overshoot commanded positions. **(b)** Data replotted to show device trajectory. For each data sample, we plotted a line segment originating at desired position and ending at actual device position. Plot is oriented according to device's orientation in space, i.e., top of plot is opposite gravity. Orientation and signs of *X* and *Y* motion axes are shown to facilitate comparison to time plots in **(a)**. Progress in time is associated with clockwise progression around circular trajectory.

Acuity Testing in Normal Subjects

Acuity was assessed in the baseline, treated, and untreated conditions (see METHODS) in 12 normal subjects experiencing simulated APN. No subject experienced dizziness or motion sickness while viewing through the activated optics. As in the previous study [6], no subject was able to identify any of the largest optotypes in the untreated condition (i.e., acuity was worse than 0.33 decimal or +0.48 logMAR). **Figure 7** shows the number of correct optotype identifications by one typical subject plotted as a function of optotype size for the treated and untreated conditions. All values represent the average of two sessions. For graphic clarity, lines connect the data points for each stimulus condition. Decimal acuity measured 1.15 in the treated condition, as opposed to 1.33 in the baseline condition. Results for all 12 subjects are summarized in **Figure 8**. Averaging over all 12 subjects, acuity measured 1.38 ± 0.29 (logMAR –0.13 ± 0.10) in the baseline condition and 1.07 ± 0.25 (–0.02 ± 0.11) in the treated condition. As such, the device restored subjects' acuities, on average, to within approximately 1 line of their true values on a Bailey-Lovie logMAR acuity chart [8].

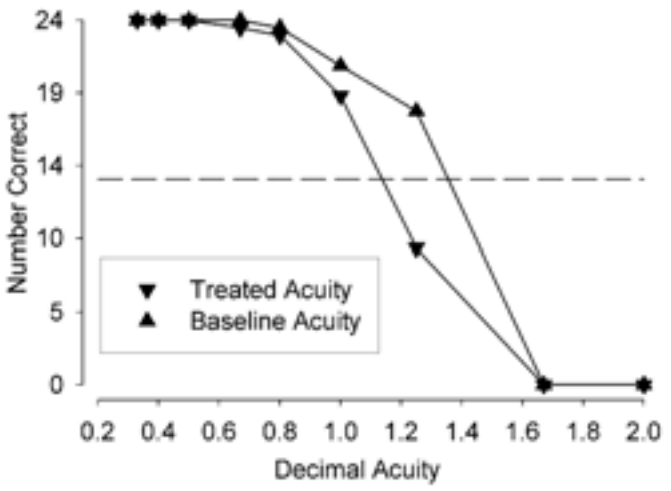

Figure 7.
Plots of number of correctly identified optotypes as functions of optotype size (expressed as decimal acuity) for one subject. Data obtained from average of two measurement sessions. Scores from "baseline" and "treated" conditions are plotted with use of upright triangles and inverted triangles, respectively. Scores from each condition are connected by straight lines for graphic clarity. Dashed line indicates criterion performance levels. Acuity for each condition was defined as optotype size at which fitted curve (not shown) crossed criterion line.

Noninterference with Normal Eye Movements

In order to be truly useful, the device should nullify the visual effects of the nystagmus but should not interfere with normal eye movements. We assessed this specificity by determining whether the device degraded acuity when subjects were required to use smooth pursuit or saccades to fixate. Five subjects underwent this testing for 1 to 2 sessions each. For these subjects, decimal acuity measured 1.64 ± 0.24 when subjects viewed the moving acuity charts through the inactivated optics versus 1.63 ± 0.24 when the optics were activated (logMAR values of –0.21 ± 0.07 and –0.21 ± 0.07, respectively). Thus, the device did not interfere significantly with the gaze-shifting eye movements required to achieve and maintain fixation of the acuity testing optotypes.

We did not explicitly study the response of the device to eye movements that compensate for head movements (i.e., the vestibulo-ocular reflex [VOR]). However, since subjects were studied without head restraint, small compensatory eye movements did occur throughout the testing. The filter is predicted to interfere with normal eye movements to the extent that their power spectra overlap the APN frequency [6], so some attenuation of VOR would have occurred and could have contributed to the small difference between acuities in the baseline and treated conditions. Subjects did not, however, complain of motion-induced oscillopsia, so the imperfect selectivity of the device should not interfere with its utility, at least during seated viewing.

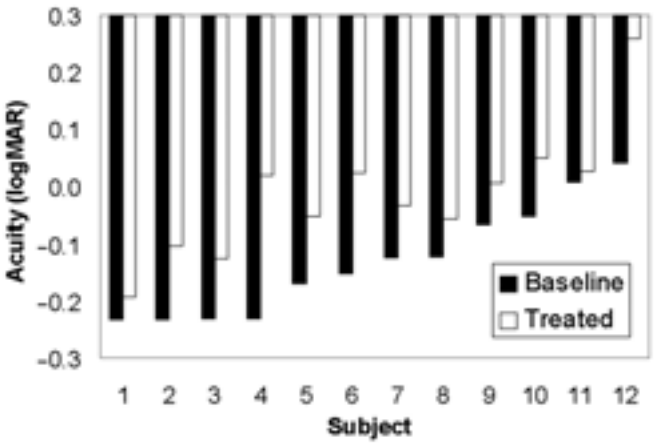

Figure 8.
Acuities measured in baseline (filled bars) and treated (open bars) conditions for all 12 subjects. Acuities are expressed as logMAR, and difference of +0.1 logMAR corresponds to worsening of acuity by one line on logarithmic acuity chart. While there was considerable variation, subjects viewing oscillating optotypes through stabilization device achieved, on average, acuity scores within one line of their scores when viewing stationary optotypes.

DISCUSSION

The three-lens image shifting device proved to be adequate to the task of restoring acuity in normal subjects experiencing simulated pendular nystagmus. With the device disabled, no subject could identify any character of the largest size we tested, a size that, if properly identified, would have corresponded to an acuity of +0.48 logMAR. With the device in operation, subjects achieved criterion accuracy at, on average, –0.02 logMAR. The difference represents at least a five-line improvement on a logarithmic acuity chart and a restoration to within one line of the subjects' performance with stationary characters.

The new image-shifting mechanism solved many of the problems we previously identified as hurdles in the path toward a practical nystagmus compensation device [9]. Chief among these problems was the need for greater fidelity in the image-shifting optics. Differences between the desired and actual image deflection cause a residual image velocity and, like the APN itself, produce oscillopsia and degrade acuity. In a previous study using motorized Risley prisms, the velocity profile of the image deflection exhibited a triangular, rather than the desired sinusoidal, profile, leading to a pronounced high-frequency oscillation in the residual image velocity perceived by the patient (see **Figure 3** of the previous study) [9]. This imperfect fidelity was believed to account for the failure of patients with 2D oscillations to benefit as expected when we operated both axes of the device, as well as the patients' preference for the device to be operated at amplitudes less than those required to fully nullify the nystagmus. In the current experiments, the improved optics executed motions that were more nearly sinusoidal (see **Figure 6(a)**), and subjects derived benefit from the device oscillating in two axes and at amplitudes equivalent to the optotype oscillation. Fidelity remained stable through oscillation rates of 10 Hz, comfortably above the maximum oscillation rate reported in multiple studies of APN in which frequency was reported [10–15].

The three-lens image-shifting optics surpassed the Risley prisms in a number of respects apart from fidelity. Whereas the Risley arrangement required powerful, AC-powered stepper motors, the new optics utilized

miniature voice coils whose total maximal current draw—about 90 mA—is entirely compatible with battery operation. Whereas the Risley prisms needed to be turned off intermittently to allow the motors to cool, the new optics could be run continuously without heating. Finally, despite the relative bulkiness of its housings, the new optics were still sufficiently light and compact to be head-mounted. With further refinements to the housing and other support components, a device tolerable for extended wear by patients should be feasible.

Experience with the prototype image-shifting device indicated a number of aspects that require further improvement. The need to reduce the weight of the mounting apparatus has already been noted. Although fidelity of the three-lens device surpassed that of the Risley prism, imperfections remain and likely account for much of the difference between subjects' acuity when viewing stationary optotypes as opposed to viewing oscillating optotypes through the active device. Fortunately, review of plots such as those shown in **Figure 6** suggest a number of ways in which the fidelity might be improved. One source of error was the tendency for the optics to overshoot the turnarounds in the command signal. These overshoots may be reduced by increasing the maximal driving current to the voice coils (or, if necessary, using more powerful voice coils), thereby increasing the ability to accelerate/decelerate the moving lens. Another source of error was the tendency for the optics to lag the command signal to varying degrees at different points in each oscillation cycle. This sort of nonlinear behavior could be reduced by replacing the current PID controller with an adaptive controller, which would map the response of the optics across the range of driving frequencies and amplitudes and use this map to optimize commands to the electromagnets so as to minimize errors [5]. Since the current PID controller is already implemented in software, replacing it with a more sophisticated algorithm may involve only programming, without the need to modify the electronics platform.

The greatest deficiency of the new optics was their being limited, for practical purposes, to angular displacements of approximately ±1°. This range would be sufficient to fully nullify the nystagmus of only selected APN patients. The exact size of that group is uncertain since the distribution of amplitudes in APN patients is unclear. Amplitude may vary from moment to moment in any given patient, and in many published studies, amplitude data are lacking, incomplete, or ambiguous (due, for instance, to failure to detail analysis methods or to specify whether the authors expressed amplitude in terms of 0-to-peak or peak-to-peak values). Based on a few studies in which clear amplitude data were supplied, only 50 to 80 percent of the patients would be fully compensated with the current optics [3,9,13,15]. Clearly, optics capable of larger amplitudes of image deflection are desirable. Increases may be achieved by increasing the power of all three lenses and/or by enlarging the moving lens armature and electromagnets so as to increase the range over which the central lens can be displaced.

CONCLUSIONS

Acuity might be improved in APN patients by a spectacle-mounted device that deflects the image of the seen world in lockstep with the involuntary eye movements. An essential component of such a device is the optical image-shifting mechanism. In order to be applicable to a nystagmus visual aid, the image-shifting mechanism must be light, accurate, suitable for battery operation, and capable of image shifting at the frequencies and amplitudes seen in APN. A three-lens image-shifting mechanism used in commercial image-stabilizing lenses has the potential to satisfy all these requirements, and, when combined with software designed to selectively track nystagmus, is capable of greatly improving acuity in normal subjects exposed to visual stimuli that simulate APN.

ACKNOWLEDGMENTS

Steven Torontali of the Design and Fabrication Center, Case Western Reserve University, assisted in disassembling the image stabilizing lens and produced the housings and head-mounted support for the rebuilt optics.

REFERENCES

1. Leigh RJ, Zee DS. The Neurology of Eye Movements. 3rd ed. New York: Oxford University Press; 1999.
2. Tomsak RL, Remler BF, Averbuch-Heller L, Chandran M, Leigh RJ. Unsatisfactory treatment of acquired nystagmus with retrobulbar injection of botulinum toxin. Am J Ophthalmol. 1995;119:489–96.

3. Leigh RJ, Rushton DN, Thurston SE, Hertle RW, Yaniglos SS. Effects of retinal image stabilization in acquired nystagmus due to neurologic disease. Neurology. 1988;38: 122–27.
4. Stahl JS, Lehmkuhle M, Wu K, Burke B, Saghafi D, Pesh-Imam S. Prospects for treating acquired pendular nystagmus with servo-controlled optics. Invest Ophthalmol Vis Sci. 2000;41:1084–90.
5. Widrow B, Stearns SD. Adaptive signal processing. Upper Saddle River, New Jersey: Prentice-Hall; 1985.
6. Smith R, Oommen B, Stahl J. Application of adaptive filters to visual testing and treatment in acquired pendular nystagmus. J Rehabil Res Dev. 2004; 41(3A):313–24.
7. Schweber B. Image stabilization shows diversity of engineering approaches. Engineering Design News. 2000 10/ 26/2000:79–82.
8. Bullimore M. Visual Acuity. In: Zadnik K, editor. The Ocular Examination: Measurements and Findings. Philadelphia: WB Saunders; 1996. p. 19–31.
9. Stahl J. Treating acquired pendular nystagmus with a servomechanical orthosis. Neurology. 1999;52 Suppl 2:A30.
10. Aschoff JC, Conrad B, Kornhuber HH. Acquired pendular nystagmus with oscillopsia in multiple sclerosis: a sign of cerebellar nuclei disease. J Neurol Neurosurg Psychiatry. 1974;37:570–77.
11. Gresty MA, Ell JJ, Findley LJ. Acquired pendular nystagmus: its characteristics, localising value and pathophysiology. J Neurol Neurosurg Psychiatry. 1982;45:431–39.
12. Starck M, Albrecht H, Pollmann W, Straube A, Dieterich M. Drug therapy for acquired pendular nystagmus in multiple sclerosis. J Neurol. 1997;244:9–16.
13. Leigh RJ, Burnstine TH, Ruff RL, Kasmer RJ. The effect of anticholinergic agents upon acquired nystagmus. A double-blind study of trihexyphenidyl and tridihexethyl chloride. Neurology. 1991;41:1737–41.
14. Averbuch-Heller L, Tusa RJ, Fuhry L, Rottach KG, Ganser GL, Heide W, et al. A double-blind controlled study of gabapentin and baclofen as treatment for acquired nystagmus. Ann Neurol. 1997;41:818–25.
15. Barton JJ, Huaman AG, Sharpe JA. Muscarinic antagonists in the treatment of acquired pendular and downbeat nystagmus: A double-blind, randomized trial of three intravenous drugs. Ann Neurol. 1994;35:319–25.

Submitted for publication October 9, 2003. Accepted in revised form December 10, 2003.